Regenerative Therapy 21 (2022) 294–306

Contents lists available at ScienceDirect

Regenerative Therapy

journal homepage: http://www.elsevier.com/locate/reth

Original Article

Appropriate pore size for bone formation potential of porous collagen type I-based recombinant peptide☆

Shoji Yamahara [a, c], Jorge Luis Montenegro Raudales [c], Yasunori Akiyama [b, c], Masaaki Ito [b, c], Ichinnorov Chimedtseren [b, c], Yoshinori Arai [e], Taku Wakita [d], Takahiro Hiratsuka [d], Ken Miyazawa [a], Shigemi Goto [a], Masaki Honda [c, *]

[a] Department of Orthodontics, School of Dentistry, Aichi Gakuin University, 2-11 Suemori-dori, Chikusa-ku, Nagoya, Aichi, 464-8651, Japan
[b] Division of Research and Treatment for Oral and Maxillofacial Congenital Anomalies, School of Dentistry, Aichi Gakuin University, 2-11 Suemori-dori, Chikusa-ku, Nagoya, Aichi, 464-8651, Japan
[c] Department of Oral Anatomy, School of Dentistry, Aichi Gakuin University, 1-100 Kusumoto-cho, Chikusa-ku, Nagoya, Aichi 464-8650, Japan
[d] Bio Science & Engineering Laboratory, FUJIFILM Corporation, 577 Ushijima, Kaisei-machi, Ashigarakami-gun, Kanagawa 258-8577, Japan
[e] Department of Oral and Maxillofacial Radiology, Nihon University School of Dentistry, 1-8-13 Kanda-Surugadai, Chiyoda-ku, Tokyo 101-8310, Japan

ARTICLE INFO

Article history:
Received 2 May 2022
Accepted 4 August 2022

Keywords:
Bone reconstruction
Bone substitute
Calvaria
Recombinant human collagen peptide
Pore size
Interconnected pore

ABSTRACT

Introduction: In this study, we developed porous medium cross-linked recombinant collagen peptide (mRCP) with two different ranges of interconnected pore sizes, Small-mRCP (S-mRCP) with a range of 100–300 μm and Large-mRCP (L-mRCP) with a range of 200–500 μm, to compare the effect of pore size on bone regeneration in a calvarial bone defect.

Methods: Calvarial bone defects were created in Sprague–Dawley rats through a surgical procedure. The rats were divided into 2 groups: S-mRCP implanted group and L-mRCP implanted group. The newly formed bone volume and bone mineral density (BMD) was evaluated by micro-computed tomography (micro-CT) immediately after implantation and at 1, 2, 3, and 4 weeks after implantation. In addition, histological analyses were carried out with hematoxylin and eosin (H&E) staining at 4 weeks after implantation to measure the newly formed bone area between each group in the entire defect, as well as the central side, the two peripheral sides (right and left), the periosteal (top) side and the dura matter (bottom) side of the defect.

Results: Micro-CT analysis showed no significant differences in the amount of bone volume between the S-mRCP and L-mRCP implanted groups at 1, 2, 3 and 4 weeks after implantation. BMD was equivalent to that of the adjacent native calvaria bone at 4 weeks after implantation. H&E images showed that the newly formed bone area in the entire defect was significantly larger in the S-mRCP implanted group than in the L-mRCP implanted group. Furthermore, the amount of newly formed bone area in all sides of the defect was significantly more in the S-mRCP implanted group than in the L-mRCP implanted group.

Conclusion: These results indicate that the smaller pore size range of 100–300 μm is appropriate for mRCP in bone regeneration.

Abbreviations: RCP, recombinant collagen peptide; mRCP, medium-cross-linked RCP; RGD, arginyl- glycyl- aspartic acid; micro-CT, micro-computed tomography; BMD, bone mineral density; ROIs, regions of interest; H&E, hematoxylin and eosin; ALP, alkaline phosphatase; TRAP, tartrate-resistant acid phosphatase; SD, standard deviation; DHT, dehydothermal treatment; CSD, critical-size defect.

☆ Present/permanent address: This work was performed in Department of Oral Anatomy, School of Dentistry, Aichi Gakuin University, 1-100 Kusumoto-cho, Chikusa-ku, Nagoya, Aichi 464-8650, Japan.

* Corresponding author. Department of Oral Anatomy, School of Dentistry, Aichi Gakuin University, 100 Kusumoto-cho, Chikusa-ku, Nagoya, Aichi 464-8650, Japan. Tel.: +81-52-751-2561; Fax.: +81-52-752-5988
E-mail address: honda-m@dpc.agu.ac.jp (M. Honda).

Peer review under responsibility of the Japanese Society for Regenerative Medicine.

https://doi.org/10.1016/j.reth.2022.08.001

1. Introduction

One of the most difficult procedures of a cleft lip and palate repair is the reconstruction of the alveolar cleft. An alveolar cleft is a bone developmental defect in the alveolar process of the maxilla [1]. Its repair allows restoring maxillary bone continuity, inducing tooth eruption, improving orthodontic treatment outcome, and reconstituting the nasal cavity floor [2–4]. Cancellous autologous bone graft harvested from the iliac crest is the most commonly used reconstruction material for alveolar cleft repair [2,4,5]. However, this procedure has several drawbacks associated with harvesting (e.g., chronic pain, infection, scar formation, hematoma, and nerve injury) [6–8]. Recently, various types of bone substitutes are being used for alveolar cleft repair [7–12]. However, the use of bone substitutes has not shown superiority compared with autologous bone grafts [13,14]. Therefore, developing novel bone substitutes is still necessary for improving the clinical outcome in the surgical repair of the alveolar cleft.

An ideal bone graft substitute should have properties such as biocompability, osteoinductivity, osteoconductivity, controlled biodegradability, ability to deliver cells at the desired site, support differentiation of regenerative cells, and the ability to promote the growth of new bone into the defect's area [7–9]. Thus, it is important to develop and evaluate candidate bone substitutes to reconstruct an alveolar cleft while reducing or preventing complications at donor site [8]. Aside from possessing biodegradable and cytophilic properties, porosity of a three-dimensional bone substitute is a highly desirable quality. A porous bone substitute can retain cells within the defect site as well as function as a substrate for tissue ingrowth and vascularization [15–19].

Fujifilm Corp. (Tokyo, Japan) has developed Cellnest®, a novel bioabsorbable recombinant protein (RCP) for medical applications based on the alpha-1 sequence (α I chain) of human collagen type I [20,21]. RCP produced by the yeast *Pichia pastoris* differs from the conventional animal collagen in the fact that there is no risk of infection, such as bovine spongiform encephalopathy, associated with it [22–24]. In addition, RCP has several favorable features as a bone substitute. First, RCP is biodegradable and bioabsorbable; thus, it does not remain in the body. Second, RCP contains 12 arginyl-glycyl-aspartic acid (RGD) motifs in a single molecule [25].

We previously conducted a series of experiments to determine whether RCP is an effective bone substitute for the regeneration of alveolar cleft bone defect [26–29]. We observed new appositional bone formation within RCP blocks upon grafting into an artificially created large bone defect at the inferior border of the rat mandible at 4 weeks after surgery. These results demonstrated that the RCP blocks are useful for repairing large bone defects [26].

To further advance our investigations in bone regeneration by RCP, we subsequently modified the formulation of RCP into porous particles to assess alveolar cleft repair, because the block shape is not compatible with the anatomical form of the human alveolar cleft. In this way, it can be easy to surgically transfer particles to the depth of the alveolar cleft. Thus, we conducted a study to clarify whether RCP particles have bone formation potential comparable to that of autologous bone chips in rat calvaria. This study showed that the bone volume formed in the RCP implanted group and the autologous bone graft group was equivalent, furthermore, the RCP particles exhibited excellent osteoconductive properties, with robust new bone formation potential, and a high degree of direct bone apposition in the calvarial bone defect [27].

Collagen-based materials require an appropriate cross-linking density for maintaining their properties because cross-linking affects cellular activities [30–35]. In addition, cross-linking helps improve the mechanical properties of materials toward degradation. However, there were no reports regarding the optimal cross-link density of RCP particles for alveolar cleft, to determine this, RCP particles with three different densities and similar pore sizes were prepared in our previous study using the palatine fissure animal experimental model [29]. The palatine fissure of a rat is a congenital bone defect that exists in the central portion of the maxilla in the oral cavity, composed of left and right sides separated by the nasal septum and has similarities to the human alveolar cleft [28,29]. When the three types of RCP particles were implanted in the rat palatine fissure, results based on micro-CT and histological analyses demonstrated that medium cross-linked RCP (mRCP) particles created a better environment for bone tissue generation compared to low or high cross-linked RCP particles. These results suggested that mRCP can be a novel bone regeneration therapy for alveolar cleft repair [29].

Interestingly, this study also revealed the significant differences in bone regeneration potential between the calvaria and palatine fissure models described above. Our data suggest that the bone-forming potential is greater in the calvaria model; this may be explained by the fact that damaged pre-existing bone has an inherent ability for regeneration as opposed to a congenital defect, which lacks a self-repair property. This was reflected in the course of the study where some degree of spontaneous healing occurred in the artificially created bone defects in the absence of bone grafts. However, the calvarial defect model is a well-established model that allows for reproducible results and precise comparison of grafted materials since it allows the researcher to control the size of the defect facilitating posterior analyses [36].

As mentioned before, porosity is an essential quality to consider in the development of bone substitutes. Similar to pore size, pore interconnectivity can also affect the smooth delivery of cells into the pores, nutrient diffusion, exchange and removal of metabolic molecules during cell culture [37]. Pores in the bone substitutes must be interconnected to allow for bone-forming cell growth, migration and nutrient flow. Therefore, controlling the pore structure, including interconnectivity is key to creating an ideal porous bone substitute [38]. In addition, the size of the interconnected pores should be in a range that facilitates cell penetration and migration during cell seeding and provides a three-dimensional microenvironment inducing cell assembly and differentiation [38]. However, the pores in the mRCP used in our previous study were not connected [27,28,30]. Therefore, in this study we developed a porous mRCP with adequate interpore connections. mRCP with two different ranges of interconnected pore sizes (100–300 μm and 200–500 μm) were prepared and the two types of mRCP were implanted in the calvarial bone defect to compare the effect of pore size on bone regeneration.

2. Materials and methods

2.1. Animals and housing

All experiments were performed using 9-week-old healthy male Sprague–Dawley rats with a bodyweight of 290–350 g (Japan SLC, Inc. Nagoya, Japan). All the rats were housed at an animal experimentation laboratory under standardized temperature and humidity, with a 12-h day/night cycle, at the Animal Research Center

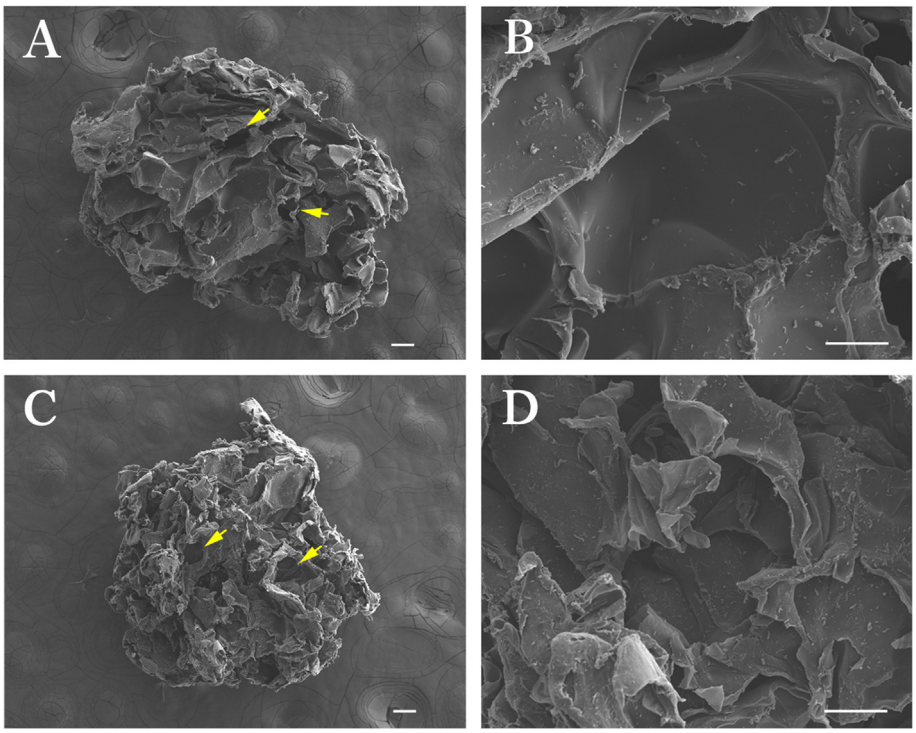

Fig. 1. Field-emission electron probe microanalyzer images of the cross sections of the two types of mRCP. L-mRCP and S-mRCP were prepared with a pore size of 200–500 μm, and 100–300 μm, respectively. L-mRCP at × 40 (A) and at × 300 (B) magnification and S-mRCP at × 40 (C) and × 300 (D) magnification. Scale bar represents 100 μm. Yellow arrows indicate interconnected pores.

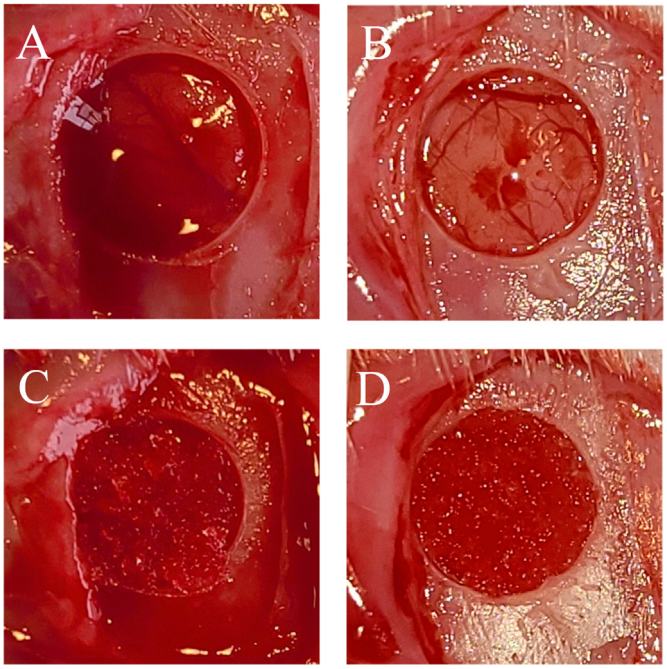

Fig. 2. Gross appearance of the 5-mm diameter bone defect made with a trephine bur in the left calvaria bone of a Sprague–Dawley rat in the (A) L-mRCP and (B) S-mRCP implanted groups. Aspect of the bone defect filled with 3 mg of (C) L-mRCP and (D) S-mRCP.

of Aichi Gakuin University. The study protocol was approved by the Animal Research Committee of the School of Dentistry, Aichi Gakuin University (approval No. AGUD412). Animal care and the experimental procedures were conducted in accordance with the Regulations on Animal Experimentation at the School of Dentistry, Aichi Gakuin University.

2.2. Preparation of mRCP with interconnected pores of different sizes

The mRCP from human type I collagen α chain was prepared as described previously (FUJIFILM, Tokyo, Japan) [20,21,25,26]. A 10 wt.% RCP solution was agitated using a dissolver in a pot cooled at 9 °C and gelled while generating bubbles in the solution. Porous sponge blocks formed by freeze-drying of the RCP gel containing bubbles were crushed into particles and cross-linked via a 4.75 h heat-dependent dehydration condensation reaction. Also, the size of each granule was kept uniform . Two types of mRCP were prepared with two different pore sizes by altering the agitating conditions. In the case of Small-mRCP (S-mRCP), agitation was performed at 2100 rpm using an agitating blade with a diameter of 40 mm. In the case of Large-mRCP (L-mRCP), agitation was performed at 1400 rpm using an agitating blade with a diameter of 40 mm. From the above, the pore sizes of S-mRCP and L-mRCP were prepared at 100–300 μm, and 200–500 μm, respectively. In addition, to perform morphological analysis of mRCP, the two types of mRCP were sprayed with an approximately 30 nm layer of carbon using a vacuum evaporator (JEE-420T; JEOL, Tokyo, Japan). The pore size images within the mRCP were taken with a field-emission electron probe microanalyzer (FE-EPMA), (JXA-8530FA, JEOL) (Fig. 1A–D). The average diameter of L-mRCP was 1171 μm and ranged from 1104 to 1265 μm (Fig. 1A and B). The average diameter of S-mRCP was 1169 μm and ranged from 1015 to 1284 μm (Fig. 1C and D).

2.3. Surgical procedure

Rats were randomly allocated into two groups and were anesthetized with 3.0% isoflurane (Mylan, Canonsburg, Pennsylvania,

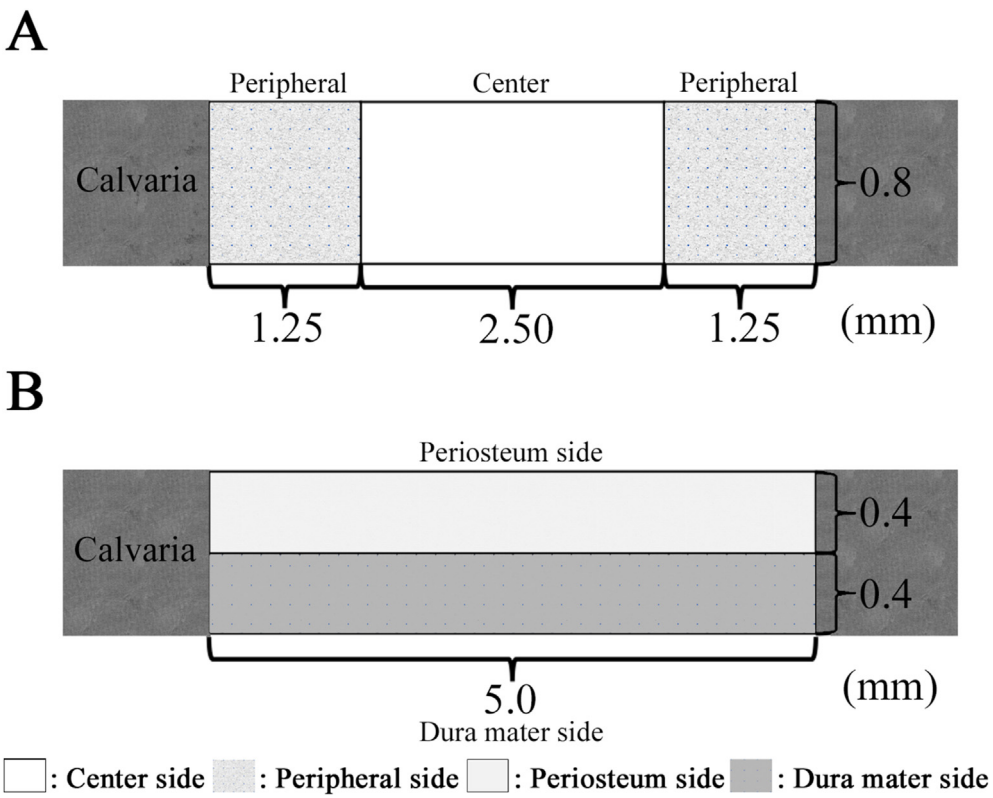

Fig. 3. Schematic representation of the rat calvarial critical-sized bone defect and histomorphometric analyses. (A) The amount of newly formed bone was calculated based on the defect width and the bone fill measurements in the peripheral area (1.25 mm × 0.8 mm) of both the sides (1.25 mm × 0.8 mm × 2) and the central area (2.5 mm × 0.8 mm). (B) The level of bone union was calculated based on the defect width and the bone fill measurements in the bottom side (dura matter side, 5.0 mm × 0.4 mm) and the top side (periosteal side, 5.0 mm × 0.4 mm).

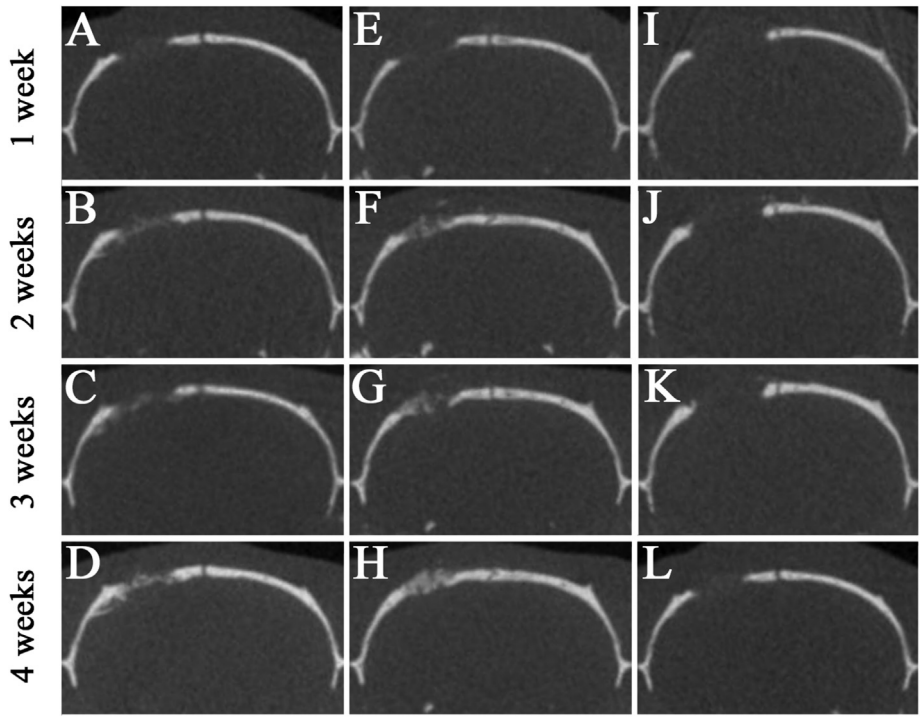

Fig. 4. Micro-CT images of the calvarial bone in the coronal plane at 1, 2, 3, and 4 weeks after implantation. (A–D) L-mRCP implanted group. (E–H) S-mRCP implanted group. (I–L) Control group.

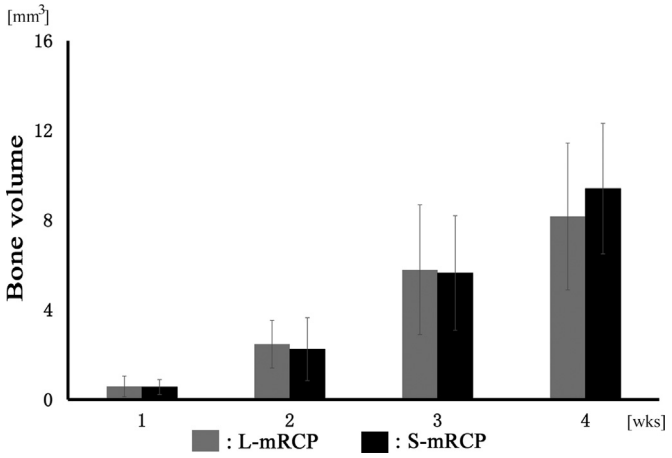

Fig. 5. Micro-CT analysis of L-mRCP and S-mRCP implanted into the calvarial bone defect for comparison of bone volume. The plots are showing the quantitative comparison of the radio-opaque areas recorded between the L-mRCP implanted group (n = 6) and the S-mRCP implanted group (n = 6) from the whole defects at week 1, 2, 3, and 4, respectively.

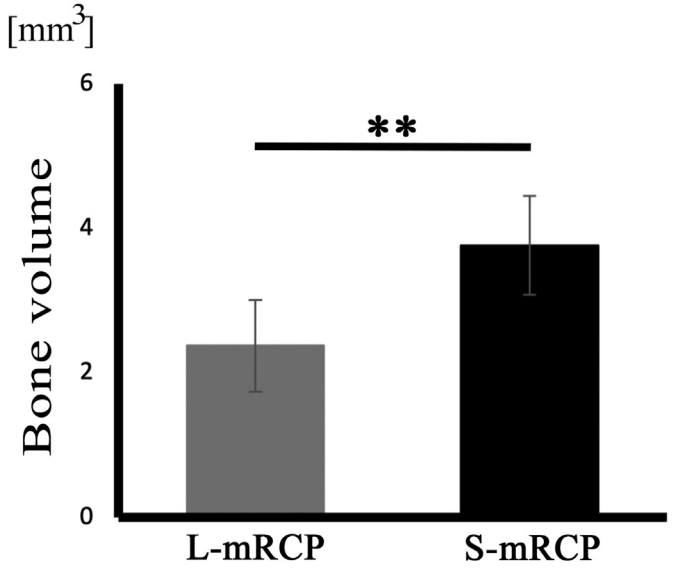

Fig. 6. Comparison of the amount of bone formation after implantation of L-mRCP and S-mRCP into the calvarial bone defect. The graph shows the bone volume of newly formed bone in the L-mRCP implanted group (n = 6) and the S-mRCP implanted group (n = 6) in the 1week interval between the 3rd and 4th week after implantation. **P < 0.01. The bars and error bars in the graph represent the mean and standard deviation (SD), respectively.

USA) in 70% nitrous oxide and 30% oxygen using a face mask and were allowed to breathe spontaneously. The head area was disinfected with povidone-iodine, a square skin incision was performed on the periosteum, and the flap was gently turned over. A periosteal flap was raised to expose the calvaria bone, and a standardized trans-osseous defect with an outer diameter of 5 mm was created unilaterally in the exposed bone using a 5.0 mm trephine bur (Meisinger, Neuss, Germany) operating at 1,500 rpm/min under continuous saline irrigation. Extreme care was exercised to avoid injury to the superior sagittal sinus and dura mater (Fig. 2A, C). Subsequently, the defect was filled with 3 mg of either L-mRCP or S-mRCR or left untreated. The rats were then grouped as follows: (1) L-mRCP implanted group (n = 6) (Fig. 2A and B); (2) S-mRCP implanted group (n = 6) (Fig. 2C and D) (3) Control group (no mRCP was implanted in the defect) (n = 3). The ablated periosteum was then repositioned, and the wounds were sutured in a single layer using 4-0 silk sutures (Ethicon Inc., GA, USA).

2.4. Micro-computed tomography (micro-CT) imaging and analysis

The total volume and bone mineral density (BMD) of the newly formed bone of both mRCP implanted groups and the neighboring native calvaria bone, were evaluated by micro-CT analysis. *In vivo*, X-ray micro-CT (Cosmo Scan GX; Rigaku Corporation, Tokyo, Japan) was used for imaging as previously described [26–29]. The exposure parameters were 18 s, 90 kV, and 100 μA. The isotropic voxel size was 45 μm. Micro-CT images were obtained from each rat immediately after surgery and at 1, 2, 3, and 4 weeks after surgery.

Bone volume was measured in the regions of interest (ROIs) from voxel images using the bone volume-measuring software, 3 by 4 viewer 2019 (Kitasenjyu Radist Dental Clinic i-View Image Center, Tokyo, Japan). The ROI size was 2.5 mm (radius) × 2.5 mm (radius) × 3.14 × 0.8 mm (depth) which covered the entire defect area created with the trephine bur. The increased bone volume in individual rats was calculated by subtracting the value of bone volume in the ROI measured immediately after surgery from the subsequent values measured at 1, 2, 3, and 4 weeks after surgery. In addition, the newly formed bone in the interval between the 1st and 2nd week, 2nd and 3rd week, and 3rd and 4th week of implantation was analyzed using the software.

Additionally, we calculated the percentage of bone volume within the bone defects using axial volume-rendered images that were obtained from 3D reconstructed micro-CT images as follows: (area of bone formation/area of ROI) × 100.

Table 1
Bone mineral density (BMD) was measured by 3 by 4 viewer 2019 software. BMD was measured in the point with the highest radiopacity by L-mRCP and the S-mRCP graft groups at 4 weeks after implantation, and compared with the neighboring native calvaria bone.

Sample	BMD (mg/cm^3)
L-mRCP graft (n = 6)	658.8 ± 18.9
S-mRCP graft (n = 6)	689.5 ± 23.1
Native calvaria bone (n = 1)	693.3

The BMD of newly formed bone was measured at 4 weeks after implantation in both mRCP implanted groups and was compared with the neighboring native calvaria bone. BMD values were measured to plot the calibration curve of the bone mineral content obtained by scanning a hydroxyapatite phantom (No.0802-08, RATOC, Tokyo, Japan) using the software, 3 by 4 viewer 2019 (Kitasenjyu Radist Dental Clinic i-View Image Center).

2.5. Tissue preparation

The animals were sacrificed in a carbon dioxide bath 4 weeks after surgery. Histological samples, including implanted sites, were harvested and fixed in 4% paraformaldehyde in phosphate-buffered saline for 24 h at 4 °C. Then, they were decalcified in 10% ethylenediaminetetraacetic acid disodium salt (Muto Pure Chemicals, Tokyo, Japan) for 8 weeks, dehydrated through a graded series of ethanol solutions, and then embedded in paraffin. The specimens were prepared as 5 μm thick sections using a microtome (Leica RM2165, Nussloch, Germany), and then stained with hematoxylin and eosin (H&E). The sections were evaluated for bone formation and integration of the reconstructed areas into the neighboring native calvaria bone, using an optical microscope. Osteoblasts and osteoclasts within the implanted area of the histological sections were visualized by alkaline phosphatase (ALP) and tartrate-

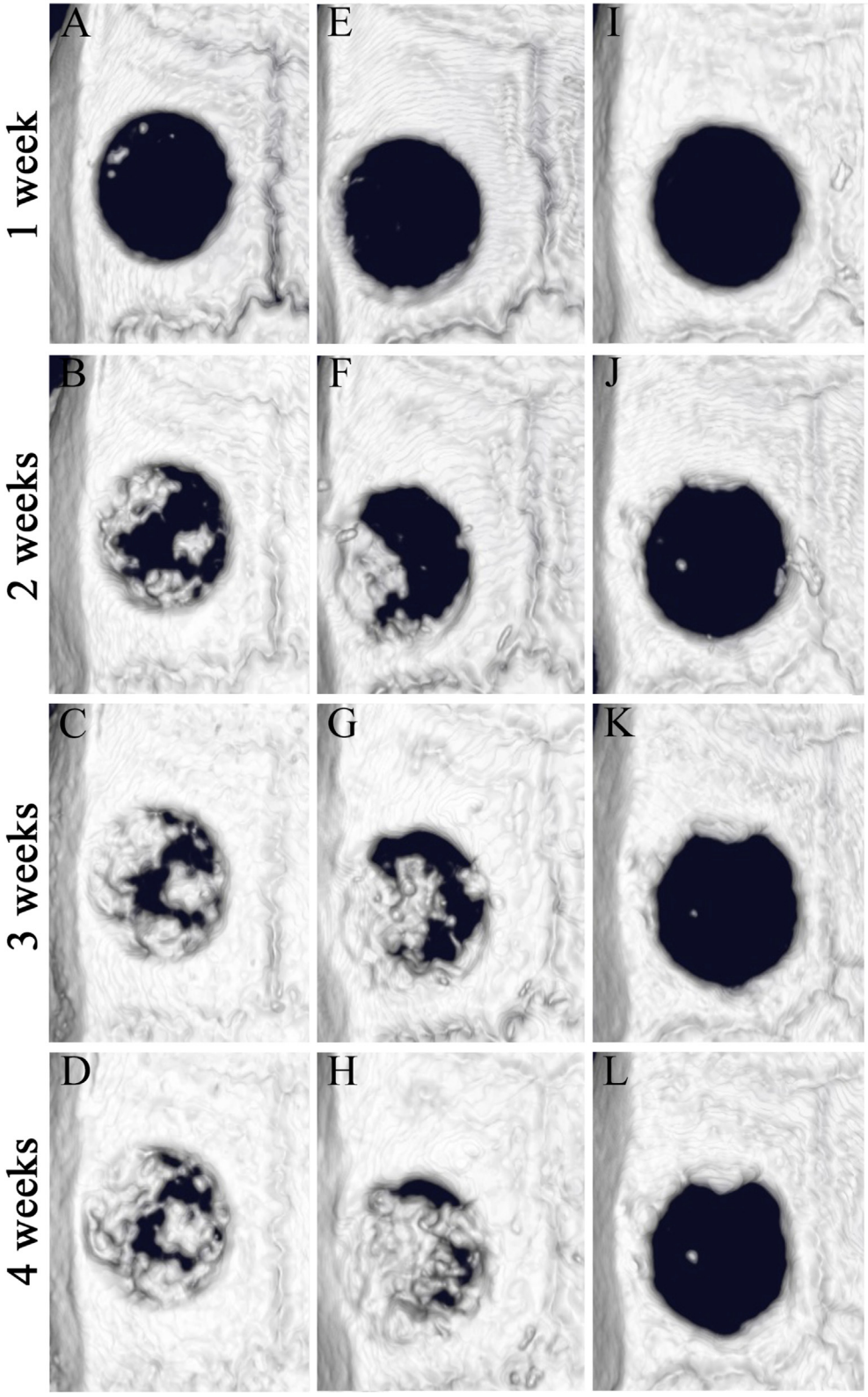

Fig. 7. Axial volume-rendered images within the calvaria bone defects obtained from 3D reconstructed micro-CT images at 1, 2, 3, and 4 weeks after implantation. (A–D) L-mRCP implanted group. (E–H) S-mRCP implanted group, and (I–L) control group.

Table 2
Percentage of bone volume within the bone defect of each group. Bone volume in the L-mRCP implanted group, S-mRCP implanted group and control group at 4 weeks after implantation was calculated by dividing the value of the bone volume in the measured ROI by the value of the ROI size, and then multiplying the result by 100.

Bone volume (%)	1w	2w	3w	4w
L-mRCP implanted group (n = 6)	3.7 ± 3.0	15.7 ± 6.8	36.9 ± 18.4	52.0 ± 21.1
S-mRCP implanted group (n = 6)	3.6 ± 2.1	14.3 ± 8.9	35.9 ± 16.1	59.9 ± 18.5
Control group (n = 3)	2.5 ± 2.0	7.4 ± 4.3	14.4 ± 7.3	18.6 ± 11.1

L, large; S, small; mRCP, medium-cross-linked recombinant peptide.

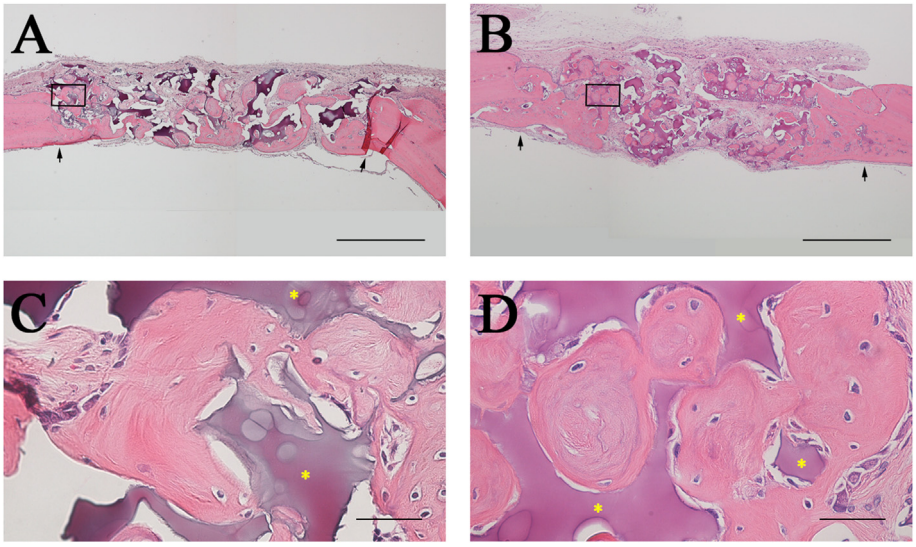

Fig. 8. Histological appearance of the calvaria bone after 4 weeks of implantation with S-mRCP and L-mRCP. Coronal plane sections were stained with hematoxylin and eosin (H&E) at 4 weeks after L-mRCP (A) and S-mRCP (B) were implanted into the calvarial bone defect. The pink-stained structure in the defect indicates newly formed bone and the purple-stained structure indicates the mRCP implant (×40). (C and D) Higher magnification (×600) of the framed area in A and B. Scale bars represent 1 mm (A and B) and 50 μm (C and D). The arrows indicate the boundary between the implanted site and the native calvarial bone.

resistant acid phosphatase (TRAP) staining, respectively (Septsapie, Tokyo, Japan). In addition, osteoclasts were also visualized by cathepsin K immunohistochemical staining using an anti-cathepsin K rabbit polyclonal antibody (Septsapie, Tokyo, Japan).

2.6. Histomorphometric analysis

For histomorphometric analysis, an image analysis software (ImageJ software, National Institutes of Health, Bethesda, MD, USA) was used to calculate the newly formed bone area within the created bone defect area (5.0 mm × 0.8 mm) of each whole histological section as described previously [27]. Statistical analyses were performed from 2 different images obtained at 4 weeks after implantation. These sections were scored via histological analysis to evaluate the level of the following aspects: newly formed bone in the entire defect area, newly formed bone at different locations in the defect site, and the bone union level (based on new bone bridging between the newly formed bone and host bone). The level of newly formed bone was calculated based on the defect width and the bone fill measurements in the peripheral area (1.25 mm × 0.8 mm) of both the sides (1.25 mm × 0.8 mm × 2) and the central area (2.5 mm × 0.8 mm) (Fig. 3A). The level of bone union was calculated based on the defect width and the bone fill measurements in the bottom side (dura matter side, 5.0 mm × 0.4 mm) and the top side (periosteal side, 5.0 mm × 0.4 mm) (Fig. 3B). In addition, the residual amount of mRCP was measured at 4 weeks after implantation, the two groups implanted with mRCP were compared and analyzed by ImageJ software.

2.7. Statistical analysis

Data are expressed as the mean and standard deviation (SD) for each group. Statistical analysis was performed using GraphPad Prism 7® (GraphPad Software, Inc., La Jolla, CA, USA). One-way analysis of variance with a Tukey–Kramer *post-hoc* test was used for intergroup comparisons. P values lower than 0.05 were considered statistically significant.

3. Results

3.1. Clinical results

Postoperative complications such as wound dehiscence, infection or severe inflammation were not observed in any of the rats. In addition, the rats showed no weight loss throughout the experimental period.

3.2. Micro-CT measurements

First, micro-CT images of the coronal plane were used to analyze the degree of hard tissue formation at the site of implantation of both mRCP groups in the calvaria bone at 1, 2, 3 and 4 weeks after implantation (Fig. 4). In both mRCP implanted groups, a slight radio-opaque area was observed at the margin of the calvaria bone defect at 1 week after implantation (Fig. 4A and E). The size of the radio-opaque areas within the bone defects gradually increased over the course of the study, and at 4 weeks after implantation, continuous or uniform or dense radiatio-opaque areas were

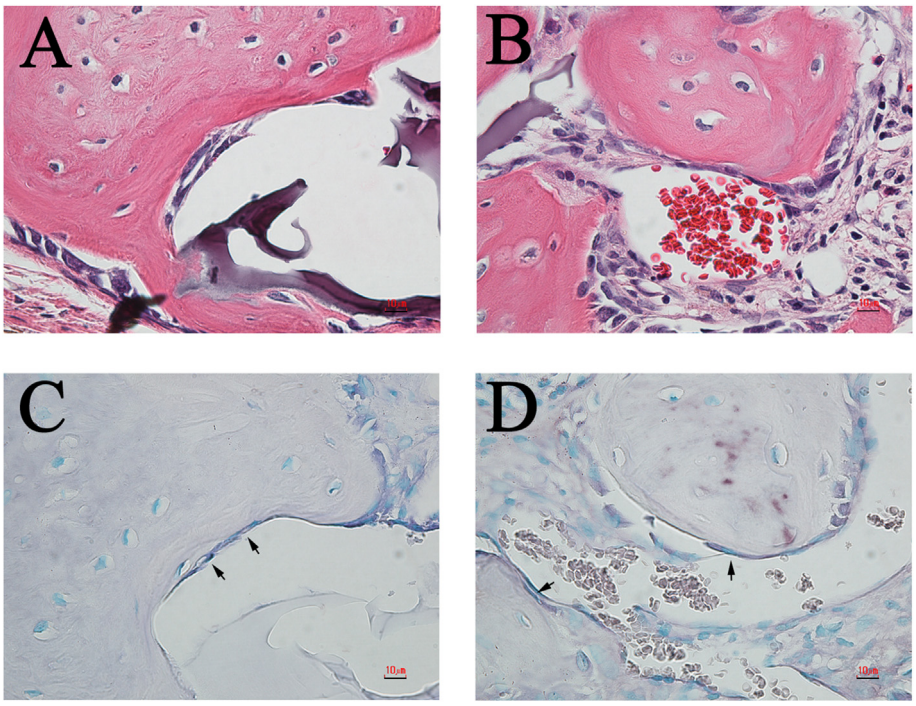

Fig. 9. Representative high-magnification (×600) images of H&E- and ALP-stained sections of the L-mRCP and S-mRCP implanted groups after 4 weeks of implantation. (A) H&E-stained section of L-mRCP implanted group at 4 weeks post-implantation. (C) Same area in (A) showing osteoblast staining with ALP (B) H&E-stained section of S-mRCP implanted group at 4 weeks post-implantation. (D) Same area in (B) showing osteoblast staining with ALP. Scale bars represent 10 μm. Arrows indicate osteoblasts.

observed to fill almost the entire area of the bone defect site (Fig. 4D and H). 4 weeks after implantation, the S-mRCP implanted group tended to show a greater radiopacity than the L-mRCP implanted group. On the other hand, in the control group, almost no radiopacity was observed in the defect even after 4 weeks of surgery (Fig. 4I–L). Since the radiopacity was observed in the both implanted groups, bone volume measurement software, 3 by 4 viewer 2019 (Kitasenjyu Radist Dental Clinic i-View Image Center, Tokyo, Japan) was used to measure the amount of regenerated bone at the bone defect site. However, there were no significant differences in the amount of bone formation between the S-mRCP and L-mRCP implanted groups at 1, 2, 3 and 4 weeks after implantation (Fig. 5).

Next, we compared the amount of bone formation gained between the implanted groups in a weekly interval. When comparing the amount of bone formation gained in the interval between the 1st and 2nd week or between the 2nd and 3rd week after implantation, no significant difference was found (data not shown). However, there was a significant difference in bone formation between the S-mRCP implanted group and the L-mRCP implanted group in the interval between the 3rd and 4th week after implantation (Fig. 6).

When the BMD of the newly formed bone was measured at 4 weeks after implantation, it was equivalent to that of the adjacent native calvaria bone. In addition, there was no significant difference in the BMD between the S-mRCP implanted group, the L-mRCP implanted group, and the native calvaria bone (Table 1). Finally, to compare the percentage of bone volume within bone defects with a diameter of 5 mm and a height of 0.8 mm, the bone defect site was observed from the axial plane using a 3D reconstructed micro-CT image (Fig. 7A–L). In the control group, even at 4 weeks post-surgery, only a small amount of newly formed bone was observed adjacent to the margin of the native calvaria bone in which the defect was created, consistent with the coronal plane image, in which almost no newly formed bone was observed in the defect area (Fig. 7L). In addition, in both the S-mRCP and L-mRCP implanted groups, the formation of regenerated bone gradually increased at 1, 2, 3 and 4 weeks after the implantation, which was consistent with the coronal plane images. Furthermore, at 4 weeks after implantation, we observed a tendency for the newly formed bone in the bone defect area to be larger in the S-mRCP implanted group than in the L-mRCP implanted group (Fig. 7D and H). Moreover, when the percentage of bone volume within the bone defect site was calculated, the S-mRCP implanted group had a higher percentage compared to the L-mRCP implanted group (Table 2).

3.3. Histological and immunohistochemical analyses

Since in both the S-mRCP and L-mRCP implanted groups newly formed bone in the defect site was observed by micro-CT imaging, we decided to compare and examine the groups by histological analysis through H&E staining (Fig. 8). When the entire bone defect in the H&E images was observed at a low magnification, the boundary between the bone defect site and the adjacent native bone was easily distinguished (Fig. 8A and B, black arrows).

The cellularized and vascularized granulation tissue formed around mRCP particles was characterized by the presence of vessels and were rich in multinucleated giant cells, especially in the bone of L-mRCP and S-mRCP implanted groups. Additionally, very limited areas of bone regeneration were observed in regions near the peripheral sides, and to a lesser extent, in the center sides of the defect of all groups.

Areas close to the defect margin showed a higher degree of direct contact between newly formed bone and mRCP.

Our previous studies have shown that in specimens implanted with mRCP, the pink-stained structures in the defect indicated newly formed bone, and the purple-stained structures indicated

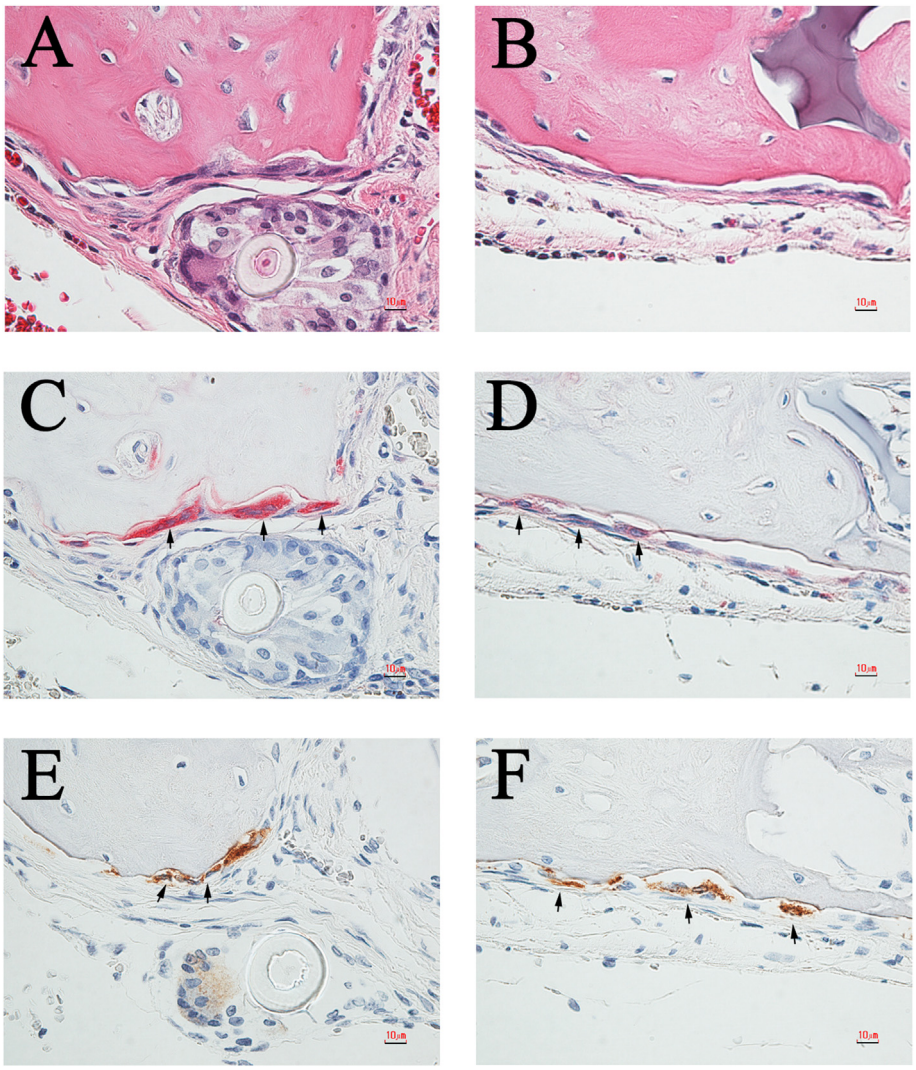

Fig. 10. Representative high-magnification (×600) images of H&E, TRAP and cathepsin K-stained sections of the L-mRCP and S-mRCP implanted groups. (A) H&E-stained section of the L-mRCP implanted group at 4 weeks post-implantation. (C) Osteoclasts were stained with TRAP at 4 weeks post-implantation. The image shows the area in A. (E) Osteoclasts were also stained with cathepsin K at 4 weeks post-implantation. The image shows the area in (A) and (C). (B) H&E-stained section of S-mRCP implanted group at 4 weeks post-implantation. (D) Osteoclasts were stained with TRAP at 4 weeks post-implantation. The image shows the area in B. (F) Osteoclasts were also stained with cathepsin K at 4 weeks post-implantation. The image shows the area in B. Scale bars represent 10 μm. Arrows indicate osteoclasts.

the implanted mRCP [27]. Further histological and immunohistochemical analyses with H&E, ALP, TRAP, and cathepsin K staining were performed to confirm that the pink-stained tissues were in fact bone (Figs. 9 and 10). In both groups, ALP-positive cells showed a polygonal morphology (Fig. 9A and B) and were observed at the site adjacent to the newly formed bone (Fig. 9C and D, black arrows). Next, resorption cavities, resembling Howship's lacunae, were observed in the pink-stained tissues in both groups (Fig. 10A and B), therefore to confirm the presence or absence of osteoclasts, TRAP/cathepsin K staining was used. TRAP-positive (Fig. 10C and D, black arrows) and cathepsin K-positive cells (Fig. 10E and F, black arrows) were found to be present near the bone resorption cavity observed by H&E staining (Fig. 10A–D, black arrows). Moreover, TRAP-positive cells and cathepsin K-positive cells were observed at almost the same site.

On the other hand, when observing the purple stained structures with H&E staining, there was an apparent tendency in which the S-mRCP implanted group showed more purple-stained regions (Fig. 8B and D). This tendency was confirmed when the total amount of the purple stained regions in the bone defects was measured using ImageJ software, and it was found that the total amount of residual S-mRCP was significantly larger than the residual L-mRCP at 4 weeks after implantation (Fig. 11).

Next, when the newly formed bone stained in pink in the total area of the bone defect was measured using ImageJ (Fig. 8A and B), the newly formed bone area was significantly larger in the S-mRCP implanted group than in the L-mRCP implanted group (Fig. 12A).

Previously, when evaluating the process of bone formation through *in vivo* experiments in which mRCP without interconnected pores was implanted in the calvaria bone defect of rats, we compared the amount of newly formed bone in the two peripheral sides (right and left) to that of the central side, as well as a comparison between the amount of newly formed bone in the periosteal (top) side and the dura matter (bottom) side of the bone defect [27,39]. Similarly, in this study, we decided to measure the amount of newly formed bone as mentioned above to evaluate the process of new bone formation (Fig. 13). In both groups, the area of newly formed bone was significantly larger in the peripheral sides adjacent to the native bone than in the central sides, and significantly larger in the dura matter (bottom) sides than in the

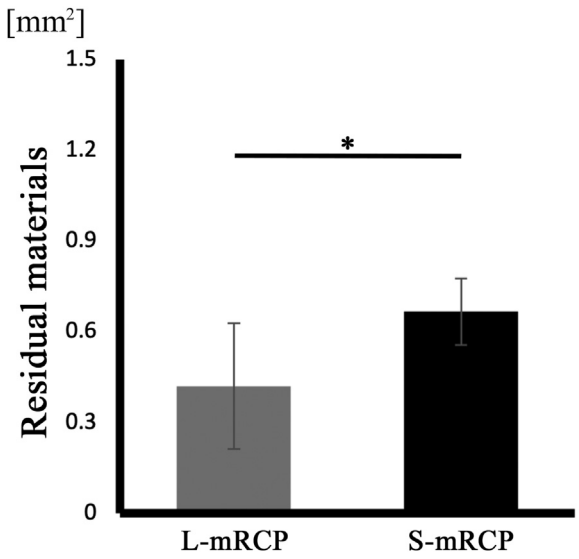

Fig. 11. Amount of residual L-mRCP and S-mRCP after 4 weeks of implantation. *P < 0.05. The graph shows the mean with SD (n = 3/group).

periosteal (top) sides (Fig. 13A–D). Furthermore, when comparing the bone formation in the central side (Fig. 12B), the two peripheral sides (right and left) (Fig. 12C), and the periosteal (top) side and the dura matter (bottom) side (Fig. 12D and E) of the defect, the amount of newly formed bone in all areas was significantly more in the S-mRCP implanted group than that of the L-mRCP implanted group.

4. Discussion

In this study, two mRCP with different interconnected pores diameters (100-300 μm and 200-500 μm) were prepared and implanted into rat calvaria defects to determine the appropriate pore size for bone regeneration. Our findings revealed that the different pore ranges did not have a significant effect in the bone density of the newly formed bone when measured by micro-CT analysis, however, histological analysis revealed that there was a significantly larger amount of bone formation induced by S-mRCP at 4 weeks after implantation. Therefore, this suggests that the interconnected pore size is an important factor to consider in the development of mRCP as a new bone substitute material.

We previously used the rat calvaria and cleft palate as evaluation sites for bone regeneration by mRCP. For the current study, we selected the calvaria as the site of implantation since data from several of our previous studies suggest that the calvarial bone has a higher bone regenerative capacity than the bone around the cleft palate, evidenced by the shorter repair period of calvarial bone defects [27,29]. Therefore, we considered that the ability to evaluate the bone-forming capacity of bone substitute materials in a short period of time would be advantageous for the development of new bone substitute materials.

Histologically, the amount of newly formed bone was larger in the S-mRCP implanted group at each defect site and in the total sum of all defect sites. When mRCP is implanted in the defect area, it contacts three major types of host tissue: the periosteum, the diploë, and the dura mater [40–42]. The blood supply from the periosteal side is relatively poor, and the source of stem cells is scarce. Since the diploë is cancellous bone, there is an abundant supply of nutrients and stem cells, and it has long been recognized that the dura plays an important role in intramembranous ossification of the calvaria [40,43,44]. In our previous study based on the mRCP with non-interconnected pores, when the implant site was divided into central and peripheral parts, to measure the amount of regenerated bone separately, it became clear that the amount of bone formation was significantly larger in the peripheral part adjacent to the diploë of the native bone than in the central part of the defect, In addition, when the bone defect was divided into the periosteal side and the dura mater side, it was also found that the bone mass was significantly larger on the dura mater side. This study showed the same results based on the mRCP with interconnected pores [27]. Taken together, mRCP with interconnected pores also can also promote bone formation without inhibiting the bone healing process in normal bone defects.

In this study, mRCP with interconnected pores were produced. When comparing the bone regeneration potential between S-mRCP and L-mRCP at each site, the defects implanted with S-mRCP had a significantly higher amount of bone formation than L-mRCP in all sites. Pore size also plays a critical role in regeneration of long bones, with experimental evidence demonstrating that bone substitutes require a pore size of at least 100 μm to supply nutrients and oxygen for cell survival and proliferation, and an optimal pore size of 200–350 μm for bone tissue ingrowth. Because bone-forming cells such as osteoblasts and osteoclasts have diameters ranging from 10 to 30 μm and 100-300 μm, respectively [45], and investigations in bone regenerative materials indicate that the pore size to facilitate cell penetration is 100–400 μm [46].

Wang et al. reported that the optimal pore size for mineralized collagen/Poly-ε-caprolactone (PCL) scaffolds in rat calvarial defect model was 130 μm [39], moreover a pore range of 100–200 μm is suitable for cell differentiation, while a pore range of 400 μm pores take time for cells to grow and fill, and that pore diameters of 290–310 μm promote bone formation [47]. Furthermore, it has been reported that bone formation is not enhanced when the pore diameter is increased to 350-800 μm [48]. Similarly, in this study, the bone formation in the L-mRCP implanted group was inferior to that of the S-mRCP implanted group. This suggests that the bone-forming potential of mRCP is reduced if the pore diameter is too large. Taken together, the pore size range of S-mRCP used in this study had more favorable cellular conditions for bone formation than the pore size range L-mRCP. This is likely to be explained by the fact that when the pore size is too large, the surface area and mechanical stability are reduced, resulting in limited cell adhesion and an insufficient level of cell-to-cell contact for proliferation, subsequently limiting bone formation [37,39].

Another reason to explain the difference of the bone-forming potential between the two types of mRCP might derive from the histological observations in which there was a tendency for the residual amount of mRCP to differ between the groups. Upon measuring the amount of residual material using ImageJ software, it became clear that the residual amount of S-mRCP was significantly larger than that of L-mRCP. This suggests that the absorption rate increased with larger pore diameters, and the absorption rate of S-mRCP and L-mRCP affected the amount of bone formation. This finding is consistent with our radiological observation where the amount bone volume formed in the interval between 3 and 4 weeks after implantation was significantly higher in the S-mRCP implanted group than in the L-mRCP implanted group. In general, it is well-known that there is an important relationship between the absorption rate of scaffolding materials used in tissue engineering and the regenerated tissue [49,50]. When the absorption rate is either too high or too low, cell proliferation and differentiation are inhibited, and thus tissue formation is negatively affected [49]. Therefore, an appropriate absorption rate is a necessary condition for an optimum scaffold material and our data suggest that the resorption rate of S-mRCP is suitable for calvarial bone regeneration. In this study we explored the effects of interconnected pore sizes in the promotion of bone formation,

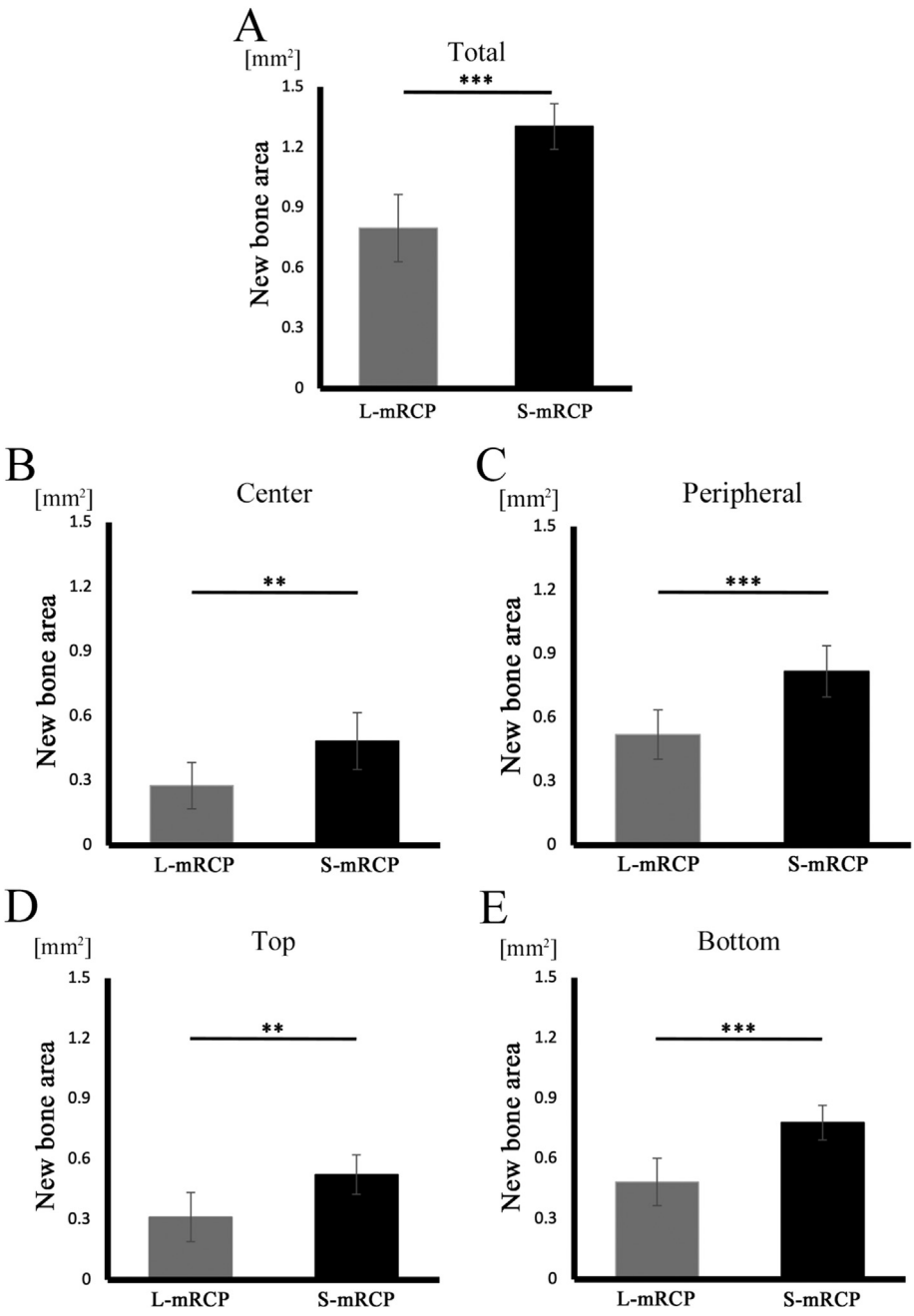

Fig. 12. Comparison of the newly formed bone area in the L-mRCP and the S-mRCP implanted groups at different locations in the defect site 4 weeks after implantation. (A) The entire bone defect (5.0 mm × 0.8 mm), (B) central bone defect (2.5 mm × 0.8 mm), (C) peripheral bone defect on both sides (1.25 mm × 0.8 mm × 2), (D) top side (5.0 mm × 0.4 mm), and (E) bottom side (5.0 mm × 0.4 mm) were measured from the entire calvarial bone defect using ImageJ software. ***P < 0.001, **P < 0.01. The graphs show the mean value with the corresponding SD (n = 3/group).

however, we think it is necessary to examine other physical properties such as mechanical strength in future investigations because it also influences the quality and quantity of newly formed bone [50–52].

Next, when the bone mineral density of the newly formed bone in both mRCP groups was measured at 4 weeks after implantation, no significant difference was observed between the S-mRCP and the L-mRCP implanted groups. Therefore, we measured the bone mineral density of the untreated calvaria bone, composed of the outer plate, diploë, and inner plate and compared it to the implanted groups. The results clarified that the bone mineral density of the bone formed after mRCP implantation was equivalent to that of the native calvaria. Further histological observations revealed a lamellar structure, and the identification of osteoblasts and osteoclasts by ALP and TRAP/cathepsin K staining, respectively, indicated that remodeling had already begun in the regenerated bone at 4 weeks, however, no significant differences in the number of osteoblasts and osteoclasts were observed between the two groups.

In summary, radiological and histological outcomes in this study showed that a pore size range of 100–300 μm was significantly more effective in calvarial bone regeneration due to a more suitable resorption rate. In the future, we plan to investigate the effectiveness of S-mRCP using a rat cleft palate model.

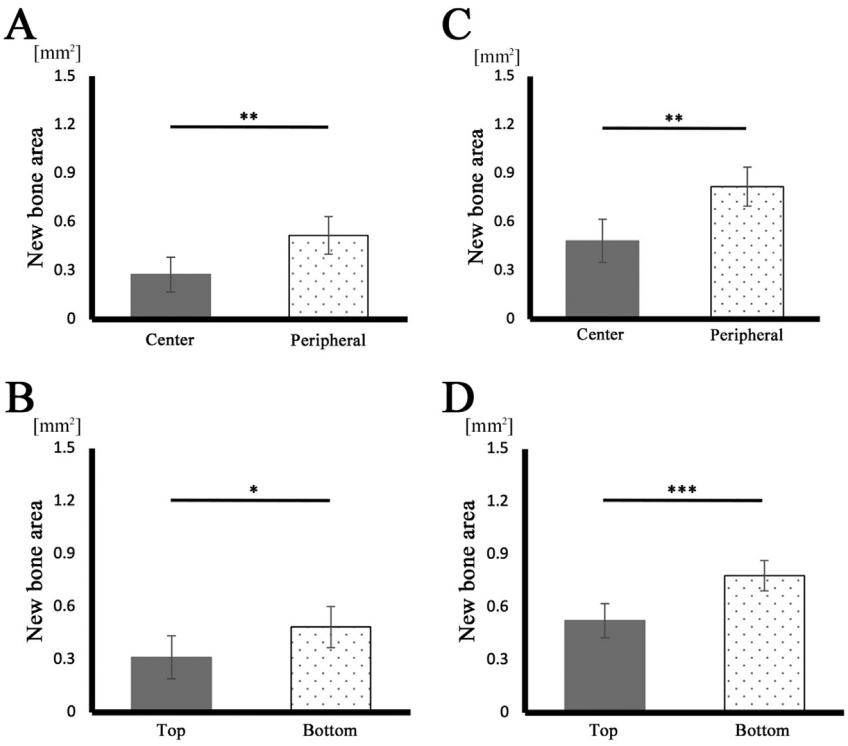

Fig. 13. Comparison of the newly formed bone area between different sites in the bone defect after 4 weeks of implantation with L-mRCP or S-mRCP. (A) The bone area of the peripheral bone defect on both sides (1.25 mm × 0.8 mm × 2) and the central bone defect (2.5 mm × 0.8 mm) were measured from the entire calvarial bone defect using ImageJ software after 4 weeks of implantation with L-mRCP. (B) The bone area of the bottom and top side (5.0 mm × 0.4 mm) of the entire calvarial bone defect (5.0 mm × 0.8 mm) were measured using ImageJ software after 4 weeks of implantation with L-mRCP. (C) The bone area of the peripheral bone defect on both sides (1.25 mm × 0.8 mm × 2) and the central bone defect (2.5 mm × 0.8 mm) were measured from the entire calvarial bone defect using ImageJ software after 4 weeks of implantation with S-mRCP. (D) The bone area of the bottom side and top side (5.0 mm × 0.4 mm) of the entire calvarial bone defect (5.0 mm × 0.4 mm) were measured using ImageJ software after 4 weeks of implantation with S-mRCP. ***P < 0.001, **P < 0.01, *P < 0.05. The graphs show the mean with SD (n = 3/group).

Disclosure

This study was funded by FUJIFILM Corporation.

Declaration of competing interest

This work was supported by the joint research expenses with FUJIFILM Corporation.

Taku Wakita, Takahiro Hiratsuka are employees of FUJIFILM Corporation.

Acknowledgments

We thank Sept Sapie CO., LTD (Tokyo, Japan) for the preparation of paraffin sections and ALP, TRAP and cathepsin K staining.

References

[1] Ali SA, Mossey P, Gillgrass T. A study model based photographic method for assessment of surgical treatment outcome in unilateral cleft lip and palate patients. Eur J Orthod 2006;28:366–72. https://doi.org/10.1093/ejo/cjl004.
[2] Bajaj AK, Wongworawat AA, Punjabi A. Management of alveolar clefts. J Craniofac Surg 2003;14:840.
[3] Raposo-Amaral CE, Denadai R, Alonso N. Three-dimensional changes of maxilla after secondary alveolar cleft repair: differences between rhBMP-2 and autologous iliac crest bone grafting. Plast Reconstr Surg Glob Open 2015;3:e451. https://doi.org/10.1097/GOX.0000000000000417.
[4] Shirani G, Abbasi AJ, Mohebbi SZ. Need for revision surgery after alveolar cleft repair. J Craniofac Surg 2012;23:378–81. https://doi.org/10.1097/SCS.0b013e318240fe7f.
[5] Forte AJV, da Silva Freitas R, Alonso N. Use of three-dimensional computed tomography to classify filling of alveolar bone grafting. Plast Surg Int 2012;2012:259419. https://doi.org/10.1155/2012/259419.
[6] Canady JW, Zeitler DP, Thompson SA, Nicholas CD. Suitability of the iliac crest as a site for harvest of autogenous bone grafts. Cleft Palate Craniofac J 1993;30:579–81. https://doi.org/10.1597/1545-1569_1993_030_0579_sotica_2.3.co_2.
[7] Chatzipetros E, Damaskos S, Tosios KI, Christopoulos P, Donta C, Kalogirou E-M, et al. The effect of nano-hydroxyapatite/chitosan scaffolds on rat calvarial defects for bone regeneration. Int J Implant Dent 2021;7:40. https://doi.org/10.1186/s40729-021-00327-w.
[8] Kang NH. Current methods for the treatment of alveolar cleft. Arch Plast Surg 2017;44:188–93. https://doi.org/10.5999/aps.2017.44.3.188.
[9] Li Y, Chen S-K, Li L, Qin L, Wang X-L, Lai Y-X. Bone defect animal models for testing efficacy of bone substitute biomaterials. J Orthop Transl 2015;3:95–104. https://doi.org/10.1016/j.jot.2015.05.002.
[10] Zerbo IR, Bronckers ALJJ, De Lange GL, Burger EH, Van Beek GJ. Histology of human alveolar bone regeneration with a porous tricalcium phosphate. Clin Oral Implants Res 2001;12:379–84. https://doi.org/10.1034/j.1600-0501.2001.012004379.x.
[11] Lu J, Descamps M, Dejou J, Koubi G, Hardouin P, Lemaitre J, et al. The biodegradation mechanism of calcium phosphate biomaterials in bone. J Biomed Mater Res 2002;63:408–12. https://doi.org/10.1002/jbm.10259.
[12] Handschel J, Wiesmann HP, Stratmann U, Kleinheinz J, Meyer U, Joos U. TCP is hardly resorbed and not osteoconductive in a non-loading calvarial model. Biomaterials 2002;23:1689–95. https://doi.org/10.1016/S0142-9612(01)00296-4.
[13] Wang Y, Bian Y, Zhou L, Feng B, Weng X, Liang R. Biological evaluation of bone substitute. Clin Chim Acta 2020;510:544–55. https://doi.org/10.1016/j.cca.2020.08.017.
[14] Liang F, Leland H, Jedrzejewski B, Auslander A, Maniskas S, Swanson J, et al. Alternatives to autologous bone graft in alveolar cleft reconstruction: the state of alveolar tissue engineering. J Craniofac Surg 2018;29:584–93. https://doi.org/10.1097/SCS.0000000000004300.
[15] Honda MJ, Shinohara Y, Hata KI, Ueda M. Subcultured odontogenic epithelial cells in combination with dental mesenchymal cells produce enamel–dentin-like complex structures. Cell Transplant 2007;16:833–47. https://doi.org/10.3727/000000007783465208.

[16] Tsuchiya S, Ohshima S, Yamakoshi Y, Simmer JP, Honda MJ. Osteogenic differentiation capacity of porcine dental follicle progenitor cells. Connect Tissue Res 2010;51:197–207. https://doi.org/10.3109/03008200903267542.
[17] Honda MJ, Yada T, Ueda M, Kimata K. Cartilage formation by serial passaged cultured chondrocytes in a new scaffold: hybrid 75:25 poly(l-lactide-ε-caprolactone) sponge. J Oral Maxillofac Surg 2004;62:1510–6. https://doi.org/10.1016/j.joms.2003.12.042.
[18] Ando Y, Honda MJ, Ohshima H, Tonomura A, Ohara T, Itaya T, et al. The induction of dentin bridge-like structures by constructs of subcultured dental pulp-derived cells and porous HA/TCP in porcine teeth. Nagoya J Med Sci 2009;71(1–2):51–62.
[19] Akita D, Morokuma M, Saito Y, Yamanaka K, Akiyama Y, Sato M, et al. Periodontal tissue regeneration by transplantation of rat adipose-derivedstromal cells in combination with PLGA-based solid scaffolds. Biomed Res 2014;35:91–103. https://doi.org/10.2220/biomedres.35.91.
[20] Nakamura K, Iwazawa R, Yoshioka Y. Introduction to a new cell transplantation platform via recombinant peptide petaloid pieces and its application to islet transplantation with mesenchymal stem cells. Transpl Int 2016;29:1039–50. https://doi.org/10.1111/tri.12810.
[21] Nakamura K, Tabata Y. A new fluorescent imaging of renal inflammation with RCP. J Contr Release 2010;148:351–8. https://doi.org/10.1016/j.jconrel.2010.09.005.
[22] Kimura Y, Inamoto T, Tabata Y. Adipose tissue formation in collagen scaffolds with different biodegradabilities. J Biomater Sci Polym Ed 2010;21:463–76. https://doi.org/10.1163/156856209X424396.
[23] Dunn RM. Cross-linking in biomaterials: a primer for clinicians. Plast Reconstr Surg 2012;130:18S. https://doi.org/10.1097/PRS.0b013e31825efea6.
[24] Mano JF, Silva GA, Azevedo HS, Malafaya PB, Sousa RA, Silva SS, et al. Natural origin biodegradable systems in tissue engineering and regenerative medicine: present status and some moving trends. J R Soc Interface 2007;4:999–1030. https://doi.org/10.1098/rsif.2007.0220.
[25] Pawelec KM, Confalonieri D, Ehlicke F, van Boxtel HA, Walles H, Kluijtmans SGJM. Osteogenesis and mineralization of mesenchymal stem cells in collagen type I-based recombinant peptide scaffolds. J Biomed Mater Res A 2017;105:1856–66. https://doi.org/10.1002/jbm.a.36049.
[26] Tateno A, Asano M, Akita D, Toriumi T, Tsurumachi-Iwasaki N, Kazama T, et al. Transplantation of dedifferentiated fat cells combined with a biodegradable type I collagen-recombinant peptide scaffold for critical-size bone defects in rats. J Oral Sci 2019;61:534–8. https://doi.org/10.2334/josnusd.18-0458.
[27] Akiyama Y, Ito M, Toriumi T, Hiratsuka T, Arai Y, Tanaka S, et al. Bone formation potential of collagen type I-based recombinant peptide particles in rat calvaria defects. Regen Ther 2021;16:12–22. https://doi.org/10.1016/j.reth.2020.12.001.
[28] Ito M, Toriumi T, Imura H, Akiyama Y, Arai Y, Natsume N, et al. Rat palatine fissure: a suitable experimental model for evaluating bone regeneration. Tissue Eng C Methods 2019;25:513–22. https://doi.org/10.1089/ten.tec.2019.0143.
[29] Ito M, Toriumi T, Hiratsuka T, Imura H, Akiyama Y, Chimedtseren I, et al. A novel bone substitute based on recombinant type I collagen for reconstruction of alveolar cleft. Materials 2021;14:2306. https://doi.org/10.3390/ma14092306.
[30] Knott L, Bailey AJ. Collagen cross-links in mineralizing tissues: a review of their chemistry, function, and clinical relevance. Bone 1998;22:181–7. https://doi.org/10.1016/S8756-3282(97)00279-2.
[31] Ammann P, Rizzoli R. Bone strength and its determinants. Osteoporos Int 2003;14:13–8. https://doi.org/10.1007/s00198-002-1345-4.
[32] McNerny EM, Gong B, Morris MD, Kohn DH. Bone fracture toughness and strength correlate with collagen cross-link maturity in a dose-controlled lathyrism mouse model. J Bone Miner Res 2015;30:455–64. https://doi.org/10.1002/jbmr.2356.
[33] Oxlund H, Barckman M, Ørtoft G, Andreassen TT. Reduced concentrations of collagen cross-links are associated with reduced strength of bone. Bone 1995;17:S365–71. https://doi.org/10.1016/8756-3282(95)00328-B.
[34] Yamauchi M, Katz EP, Mechanic GL. Intermolecular crosslinking and stereospecific molecular packing in type I collagen fibrils of the periodontal ligament. Biochemistry 1986;25:4907–13. https://doi.org/10.1021/bi00365a027.
[35] Kuroshima S, Kaku M, Ishimoto T, Sasaki M, Nakano T, Sawase T. A paradigm shift for bone quality in dentistry: a literature review. J Prosthodont Res 2017;61:353–62. https://doi.org/10.1016/j.jpor.2017.05.006.
[36] Gomes PS, Fernandes MH. Rodent models in bone-related research: the relevance of calvarial defects in the assessment of bone regeneration strategies. Lab Anim 2011;45:14–24. https://doi.org/10.1258/la.2010.010085.
[37] Murphy CM, Haugh MG, O'Brien FJ. The effect of mean pore size on cell attachment, proliferation and migration in collagen–glycosaminoglycan scaffolds for bone tissue engineering. Biomaterials 2010;31:461–6. https://doi.org/10.1016/j.biomaterials.2009.09.063.
[38] Zhang Q, Lu H, Kawazoe N, Chen G. Pore size effect of collagen scaffolds on cartilage regeneration. Acta Biomater 2014;10:2005. https://doi.org/10.1016/j.actbio.2013.12.042. –13.
[39] Wang S, Yang Y, Koons GL, Mikos AG, Qiu Z, Song T, et al. Tuning pore features of mineralized collagen/PCL scaffolds for cranial bone regeneration in a rat model. Mater Sci Eng C 2020;106:110186. https://doi.org/10.1016/j.msec.2019.110186.
[40] Gosain AK, Santoro TD, Song L-S, Capel CC, Sudhakar PV, Matloub HS. Osteogenesis in calvarial defects: contribution of the dura, the pericranium, and the surrounding bone in adult versus infant animals. Plast Reconstr Surg 2003;112:515–27. https://doi.org/10.1097/01.prs.0000070728.56716.51.
[41] Mabbutt LW, Kokich VG. Calvarial and sutural re-development following craniectomy in the neonatal rabbit. J Anat 1979;129:413–22.
[42] Reid CA, McCarthy JG, Kolber AB. A study of regeneration in parietal bone defects in rabbits. Plast Reconstr Surg 1981;67:591–6.
[43] Hobar PC, Schreiber JS, McCarthy JG, Thomas PA. The role of the dura in cranial bone regeneration in the immature animal. Plast Reconstr Surg 1993;92:405–10. https://doi.org/10.1097/00006534-199309000-00003.
[44] Kpelao E, Kader MAE, Anthony BK, Alain A, Agbeko D, Hobli A, et al. Technique of granulation tissue genesis from diploe. Mod Plast Surg 2018;8:9. https://doi.org/10.4236/mps.2018.82002.
[45] Tiedemann K, Le Nihouannen D, Fong JE, Hussein O, Barralet JE, Komarova SV. Regulation of Osteoclast Growth and Fusion by mTOR/raptor and mTOR/rictor/Akt. Front Cell Dev Biol 2017;5.
[46] Draenert K, Draenert M, Erler M, Draenert A, Draenert Y. How bone forms in large cancellous defects: critical analysis based on experimental work and literature. Injury 2011;42:S47–55. https://doi.org/10.1016/j.injury.2011.06.007.
[47] Nathanael AJ, Oyane A, Nakamura M, Sakamaki I, Nishida E, Kanemoto Y, et al. In Vitro and in vivo analysis of mineralized collagen-based sponges prepared by a plasma- and precursor-assisted biomimetic process. ACS Appl Mater Interfaces 2017;9:22185–94. https://doi.org/10.1021/acsami.7b04776.
[48] Roosa SMM, Kemppainen JM, Moffitt EN, Krebsbach PH, Hollister SJ. The pore size of polycaprolactone scaffolds has limited influence on bone regeneration in an in vivo model. J Biomed Mater Res A 2010;92A:359–68. https://doi.org/10.1002/jbm.a.32381.
[49] Guo Y, Chen Z, Wen J, Jia M, Shao Z, Zhao X. A simple semi-quantitative approach studying the in vivo degradation of regenerated silk fibroin scaffolds with different pore sizes. Mater Sci Eng C 2017;79:161–7. https://doi.org/10.1016/j.msec.2017.05.008.
[50] Zhang L, Liu X, Li G, Wang P, Yang Y. Tailoring degradation rates of silk fibroin scaffolds for tissue engineering. J Biomed Mater Res A 2019;107:104–13. https://doi.org/10.1002/jbm.a.36537.
[51] Partlow BP, Tabatabai AP, Leisk GG, Cebe P, Blair DL, Kaplan DL. Silk fibroin degradation related to rheological and mechanical properties. Macromol Biosci 2016;16:666–75. https://doi.org/10.1002/mabi.201500370.
[52] Rosso F, Marino G, Giordano A, Barbarisi M, Parmeggiani D, Barbarisi A. Smart materials as scaffolds for tissue engineering. J Cell Physiol 2005;203:465–70. https://doi.org/10.1002/jcp.20270.